

DyLoc: Dynamic Localization for Massive MIMO Using Predictive Recurrent Neural Networks

Farzam Hejazi

Department of Electrical
and Computer Engineering
University of Central Florida
Orlando, USA
farzam.hejazi@ucf.edu

Katarina Vuckovic

Department of Electrical
and Computer Engineering
University of Central Florida
Orlando, USA
kvuckovic@knights.ucf.edu

Nazanin Rahnavard

Department of Electrical
and Computer Engineering
University of Central Florida
Orlando, USA
nazanin.rahnavaard@ucf.edu

Abstract—This paper presents a data-driven localization framework with high precision in time-varying complex multipath environments, such as dense urban areas and indoors, where GPS and model-based localization techniques come short. We consider the angle-delay profile (ADP), a linear transformation of channel state information (CSI), in massive MIMO systems and show that ADPs preserve users’ motion when stacked temporally. We discuss that given a static environment, future frames of ADP time-series are predictable employing a video frame prediction algorithm. We express that a deep convolutional neural network (DCNN) can be employed to learn the background static scattering environment. To detect foreground changes in the environment, corresponding to path blockage or addition, we introduce an algorithm taking advantage of the trained DCNN. Furthermore, we present *DyLoc*, a data-driven framework to recover distorted ADPs due to foreground changes and to obtain precise location estimations. We evaluate the performance of *DyLoc* in several dynamic scenarios employing DeepMIMO dataset [1] to generate geo-tagged CSI datasets for indoor and outdoor environments. We show that previous DCNN-based techniques fail to perform with desirable accuracy in dynamic environments, while *DyLoc* pursues localization precisely. Moreover, simulations show that as the environment gets richer in terms of the number of multipath, *DyLoc* gets more robust to foreground changes.

Index Terms—Data-driven Localization, massive MIMO, Deep Learning, Dynamic Environments, Frame Prediction

I. INTRODUCTION

With the expansion of location-based services such as peer-to-peer ride sharing, local search-and-discovery mobile apps, navigation services, store locators, autonomous driving, and urban unmanned aerial systems (UAS) traffic management, the demand for highly-accurate positioning technologies is growing [2]. When the environment is free from strong multipath (mainly outdoor environments), localization can be considered mostly a solved problem [3]. Nonetheless, localization in harsh multipath environments (mainly indoors and dense urban areas) has remained under extensive investigation [4].

For environments where line of sight (LOS) is dominant and multipath is scarce, various localization techniques have been proposed in the literature, majority of which are model-based. In these environments, physical models can describe the scattering surrounding quite well. These techniques mainly employ received signal strength indicator (RSSI), time of arrival (ToA), time difference of arrival (TDoA) and angle

of arrival (AOA) measurements to pursue localization [5]–[14]. One major issue with model-based techniques is that they normally require measurements of those parameters from multiple anchor nodes which may not be available in every environment. To address shortfalls of model-based techniques and to tackle localization for complex multipath environments, several data driven approaches have been proposed. Data-driven localization techniques are mainly called *fingerprinting-based localization* [15]. This type of localization generally constitutes gathering a dataset of a geo-tagged communication parameter (e.g. RSSI or channel state information (CSI)) all over the environment and training a neural network based on the dataset for online localization. Unfortunately, the data-driven approach has also failed to solve the problem of localization in complex multipath environments thus far. Data-driven approaches are highly dependent of an exorbitant campaign of gathering a geo-tagged dataset. Moreover, they need several hours of training. During these two relatively prolonged procedures, it is probable that the environment changes and the dataset becomes invalid [16]. Some efforts have been conducted to taper the required dataset and reduce the training time [17]; however, in the best-case scenario they could reduce the initial required time to a couple of hours while these environments can change in a couple of seconds. Furthermore, it is almost impossible to gather data for every possible dynamic scenario and retrain the network.

Massive multi input multi output (MIMO) is a technique in wireless networks that utilizes numerous antennas mainly at base stations to take advantage of multipath effect to spatially multiplex users [18]. Massive MIMO is considered a core technology behind the revolution in ultra-high speed communications promised by 5G cellular networks [19]. To enable spatial multiplexing, base stations must identify the propagation environment from their antennas to the users’ antennas. This task is routinely conducted by measuring CSI. When measured perfectly, CSI preserves all information about scattering, fading, delays and power decay of the channel. Due to the rich information contained in CSI, it is considered an integral parameter for single-site fingerprinting-based localization. Vieira et. al. considered using a deep convolutional neural network (DCNN) trained by angle delay profiles (ADPs) for

localization for the first time in the literature [20]. Viera shows that in addition to memorizing the dataset, the trained DCNN can generalize localization to unknown location within the environment. Sun et. Al. trained two different DCNNs to pursue the localization task. The first network is similar to the regression network proposed by Viera. The second network incorporates two different blocks, the first block is a classification DCNN that defines to which grid cell the user location belongs, and the second block uses a weighted K-nearest neighbor (WKNN) algorithm to find the user location within the cell precisely [21]. In [22], the authors design input features to make them robust to CSI impairments. They consider an autocorrelated version of CSI as the input to the CNN. In [23], De Bast et. al. showed that CNN trained using CSI performs with centimeter accuracy in a static indoor environment. However, when a person is walking in the room the error increased by ten folds or more. To the best of our knowledge, this is the only work that examines the effect of dynamic scenarios on the accuracy of localization via a CNN trained using CSI. Unfortunately, the available literature mostly considers static scenarios and ignores the dynamic nature of complex scattering environments. To address this shortcoming, in our work, we mainly focus on addressing localization in *dynamic scenarios* leveraging a data-driven approach. To the best of authors' knowledge, this work is the first attempt to tackle localization in complex dynamic environments with a data-driven perspective.

Deep learning has shown outstanding performance in the field of computer vision (CV) so far. Among all various topics in the CV context, video surveillance, video frame prediction, video foreground and anomaly detection tackle highly dynamic problems [24]–[26]. In our work, we adopt some ideas from frame prediction literature to address data-driven localization in dynamic environments. First, we prove that time-series of ADPs preserves users' movements assuming a static environment (the static environment is referred to as background (BG)). Consequently, it leads us to infer predictability of the next frame on an ADP temporal sequence based on previous frames using a predictive recurrent neural network. We model changes in the environment by LOS blockage, none LOS (NLOS) blockage, and NLOS addition, referred as foreground (FG). We propose an algorithm to discriminate between those ADPs which are accurate and those distorted by FG. Consequently, we propose *DyLoc* to recover distorted ADPs and *to estimate* the user location incorporating a WKNN block with a predictive recurrent neural network (PredRNN) block. To examine the performance of DyLoc we consider an indoor and an outdoor environments utilizing DeepMIMO dataset [1]. We show that a trained CNN fails to estimate user location with acceptable accuracy in dynamic environments while the proposed technique can estimate user location with a decent accuracy. The main contributions of our work can be encapsulated as follow:

- Proving that a time-series of ADPs can preserve users' movements

- Showing ADP can be predicted based on previous frames of the ADP time-series
- Modeling changes in the environment as LOS blockage, NLOS blockage, and NLOS addition
- Proposing DyLoc, a novel localization algorithm, that includes two steps: (i) an algorithm to detect distorted ADPs, and (ii) an algorithm to recover distorted ADPs and to estimate users' location utilizing PredRNN and WKNN techniques.

The rest of the paper is organized as follows. In Section II, we present the considered system and channel model and define ADP. We introduce motion preservation property of ADP in Section III-A. In Section III-B, we express how we can model a dynamic propagation environment, where propagation paths can be blocked or added at anytime. We present a new prospective toward fingerprint gathering campaigns in Section IV. In Section V, we introduce DyLoc to tackle the localization task in complex environments. In Section VI, we examine the performance of the proposed technique via various simulations. Finally, we conclude the paper in Section VII.

II. SYSTEM AND CHANNEL MODEL

Assume we require to localize a single user, utilizing a single base station (BS) of a typical MIMO-Orthogonal frequency-division multiplexing (OFDM) wireless network. For the ease of exposition and similar to [27], we suppose that the BS is equipped with a uniform linear array (ULA), with half wavelength spacing between two adjacent antennas, and a user's device has a single omni-directional antenna. The BS has N_t antennas, and uses OFDM signaling with N_c sub-carriers. We assume a geometric channel model between the BS and the user with C distinguishable clusters. Moreover, each cluster constitutes R_C distinguishable paths. Each path can be characterized by a delay $\tau_m^{(k)}$, $k \in \{1, \dots, C\}$, $m \in \{1, \dots, R_C\}$, an AOA to the BS's antenna $\theta_m^{(k)}$ and a complex gain $\alpha_m^{(k)}$ [27]. Assuming a wide-band OFDM system, $\tau_m^{(k)} = n_m^{(k)} T_s$, where T_s and $n_m^{(k)}$ denote the sampling duration and the sampled delay belonging to the path m of the cluster k , respectively [21]. Assuming these parameters, channel frequency response (CFR) for each sub-carrier l can be written as [28]

$$\mathbf{h}[l] = \sum_{k=1}^C \sum_{m=1}^{R_C} \alpha_m^{(k)} e^{j\theta_m^{(k)}} e^{-j2\pi \frac{l n_m^{(k)}}{N_c}}, \quad (1)$$

where j denotes the imaginary unit and $e^{j\theta}$ denotes the array response vector of the ULA given by

$$\mathbf{e}(\theta) = [1, e^{-j2\pi \frac{d \cos(\theta)}{\lambda}}, \dots, e^{-j2\pi \frac{(N_t-1)d \cos(\theta)}{\lambda}}]^T, \quad (2)$$

where d is the gap between two adjacent antennas and λ is the wavelength. Thus, the overall CFR matrix of the channel between the BS and the user can be expressed as

$$\mathbf{H} = [\mathbf{h}[1], \dots, \mathbf{h}[N_c]]. \quad (3)$$

This matrix commonly is referred to as CSI in the literature.

Angle Delay profile (ADP) is a linear transformation of the CSI computed by multiplying it with two discrete Fourier transform (DFT) matrices. Let us define the DFT matrix $\mathbf{V} \in \mathbb{C}^{N_t \times N_t}$ as

$$[\mathbf{V}]_{z,q} \triangleq \frac{1}{\sqrt{N_t}} e^{-j2\pi \frac{(z(q - \frac{N_t}{2}))}{N_t}},$$

and $\mathbf{F} \in \mathbb{C}^{N_c \times N_c}$ as

$$[\mathbf{F}]_{z,q} \triangleq \frac{1}{\sqrt{N_c}} e^{-j2\pi \frac{zq}{N_c}}.$$

Then ADP matrix \mathbf{G} is defined as [21]

$$\mathbf{G} = \mathbf{V}^H \mathbf{H} \mathbf{F}. \quad (4)$$

Now, let us define $[\mathbf{A}]_{z,q} = |\mathbf{G}_{z,q}|$, where $|\cdot|$ denotes absolute value. Throughout this paper, we refer to \mathbf{A} as ADP. When measured perfectly, CSI is a very rich data and preserves all scattering characteristics of the channel. However, when depicted in its raw format it is completely meaningless. On the other hand, referring to [29], the (z, q) element of the ADP represents the absolute gain of z^{th} AOA and q^{th} delay as illustrated in Fig. 1. Therefore, we can simply make sense of ADP as a visual representation of all distinguishable paths between the user and the BS. For example, we can deduct from Fig. 1 that there is a LOS path cluster with AOA around 18° and approximately 10^{-8} s delay, and there are eight NLOS clusters between the user and the BS. Using ADP, we can cast the localization problem as a pattern recognition problem and take advantage of the rich literature of deep learning applications in CV [21].

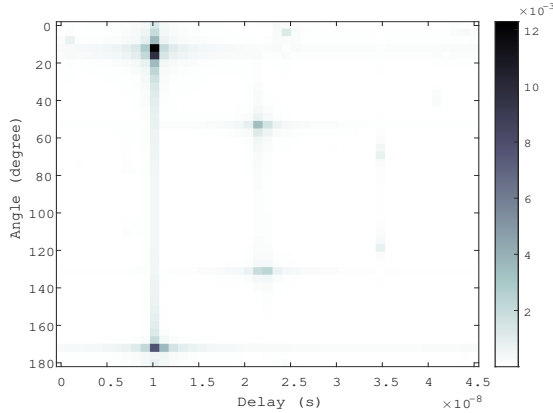


Fig. 1: A sample ADP image. Each pixel represents the absolute gain of the path with the corresponding AOA and the delay. Each "++"-like shape in the image shows a path cluster between the BS and the user.

III. SCATTERING ENVIRONMENT

In this section, we discuss static and dynamic environments and how a user's motion reflects on ADP. We will show that when a user moves in a continuous track in the location domain, all paths in ADP also move in a continuous track, assuming a totally static environment. Moreover, we discuss dynamic changes in the environment and how we can model their effects on scatterings.

A. Static Environment

First, let us define what we mean by a static environment. **Definition 1. Static environment** is an environment including a user and at least one base station, in which nothing other than the user can move and all the materials of the surfaces remain the same within the environment. In this environment, scattering (influenced by propagation paths, decays, and delays) remains unchanged. Moreover, the user's motion does not affect the scattering and does not block or add any path, while it may change visible paths between the BS and the user.

Theorem 1. Let us consider a static environment where the user's movement does not change the paths between the BS and the user. Given a static environment, assume the user movement does not change the visible paths between the BS and the user. If user's position shifts by some very small positive amount δd , changes in delay of paths are limited to the following bounds

$$\delta\tau_m^{(k)} \leq \frac{\delta d}{v_c}; \quad \forall k \in \{1, \dots, C\}, \forall m \in \{1, \dots, R_C\}, \quad (5)$$

where v_c denotes the speed of light and $\delta\tau_m^{(k)}$ denotes changes in the delay of the path m of cluster k . Further, the following bound on the path AOA shift holds for any $\alpha > 1$

$$\lim_{\delta d \rightarrow 0} \delta\theta_m^{(k)} \leq \alpha \frac{\delta d}{d_m^{(k)}}, \quad \forall k \in \{1, \dots, C\}, \forall m \in \{1, \dots, R_C\}, \quad (6)$$

where $\delta\theta_m^{(k)}$ and $d_m^{(k)}$ are changes in the AOA and the length of the path m of cluster k , respectively.

Proof. When the user's position changes by δd , the length of each path from the BS to the user (LOS and NLOS) will change the same or less, thus the change in the delay is limited to $\frac{\delta d}{v_c}$.

Assuming LOS path (path 1 in Fig. 2), change in the angle of the path is the maximum if the movement is perpendicular to the path. Thus, assuming the movement is perpendicular to the LOS, then $\tan(\delta\theta) = \frac{\delta d}{d_{path}}$, where d_{path} is the length of the path from the BS to the user and $\delta\theta$ is the change in AOA of signal from the user to the BS. Considering $\lim_{x \rightarrow 0} \tan(x) \rightarrow x$, for any $\alpha > 1$ there is a δd close enough to zero such that $\delta\theta_m^{(k)} \leq \alpha \frac{\delta d}{d_m^{(k)}}$.

Referring to [30], every NLOS path from the BS to the user, can be considered as a LOS path from a virtual BS to the user, with the same length (Fig. 2). Thus, (6) holds for a NLOS path as well. \square

Referring to Theorem 1, we can infer that, given a static environment and fixed paths between the BS and the user, any continuous user's movement in the location domain will result in a continuous movement in the angle-delay domain. In other words, when the user moves within the environment, all paths in the angle-delay domain start moving in a continuous track. Consequently, if we cascade consecutive ADPs to form a time-series data, the sequence is highly correlated temporally.

Theorem 1 expresses that if a path exists in the ADP, it moves in a continuous track when the user moves. In

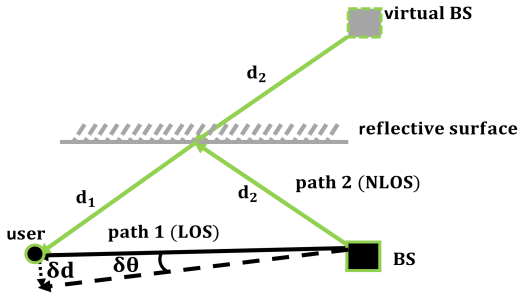


Fig. 2: LOS and NLOS paths geometry. The NLOS path can be considered as a LOS path from a virtual BS located at the reflection of the BS with respect to the reflective surface.

In addition to path motion, even in a static environment, it is possible that some paths dissipate and some new visible paths emerge during the user movement. Referring to [29], ADP is highly correlated in location domain and similarities between the ADPs decrease smoothly with respect to their physical distances. Thus, emergence and dissipation of paths occur very smoothly during the user movement. Hence, the following conclusion can be inferred:

Collorary 1: Assuming a static environment, consecutive frames of time-series of the user measured ADPs show a continuous movement for all paths between the BS and the user.

This conclusion leads us to the idea that it may be possible to predict future ADP frames based on the time-series of past frames.

B. Dynamic Behaviour of The Environment

Till now, we have discussed that a time-series of ADPs belonging to a certain user are highly correlated temporally, assuming a static environment. Nonetheless, complex scattering environments are normally highly dynamic. This means that several objects can move into and out of them and can change the scattering environment quickly and thoroughly. Dynamic changes in the environment result in the following changes in the static scattering environment:

- 1) **LOS blockage:** a new object blocks the LOS path between the user and the BS.
- 2) **NLOS blockage:** a new object blocks some NLOS paths between the user and the BS.
- 3) **NLOS addition:** scattering from surfaces of a new object adds some NLOS paths between the user and the BS.

We assume that all objects and surfaces belonging to the static environments stay fixed and unchanged, therefore a LOS path already blocked by the static environment cannot get unblocked by the dynamic movements inside the environment.

IV. RETHINKING OF FINGERPRINT GATHERING CAMPAIGNS

To form a dataset of geo-tagged CSIs (or any other communication parameter), previous studies have generally considered measuring CSI at several locations inside a static environment. Such campaigns may be ineffective for user

localization in dynamic scenarios in the first place, since few movements inside the environment may invalidate the whole dataset quickly. In this work, we introduce a new perspective toward these data gathering campaigns that can picture them as an integral part of any data-driven dynamic localization framework. In fact, by measuring CSI around a static environment, we map spatial distribution of all propagation paths within the static environment. It is like recording video footage from the whole static environment from the BS point of view. Such a footage can reveal all LOS and NLOS paths from any point inside the environment to the BS (or vice versa) in visible light band. Similarly, such measurement campaigns in radio frequency bands help us to understand the underlying scattering environment thoroughly, from the BS point of view. In the video processing literature, the underlying static environment and the changing environment are called "background" and "foreground", respectively. Here, we mimic the same pattern. In fact, measurement campaigns are quite obliging for understating the static scattering environment. Once the measurements are complete, we can utilize our understanding of BG to detect FG and employ proper algorithms to track changes and recover the true BG. Such a prospective toward fingerprinting, in conjunction with meaningful representation of the environment via ADP images, enables us to cast dynamic fingerprinting problem (or any other wireless communication problem that should deal with a dynamic scattering environment) as a video processing problem. Eventually, this redefinition enables us to take advantage of the rich literature of video surveillance, video frame prediction, and video foreground and anomaly detection in the context of computer vision to tackle wireless communication problems in dynamic environments.

V. DYLOC: DYNAMIC LOCALIZATION VIA FINGERPRINTING

In this section, we introduce our proposed localization framework for dynamic environments. Suppose a user is moving inside an environment where there is a BS utilizing massive MIMO technology for communication as defined in Section II. Some of the measured CSIs may get affected by FG and get distorted compared to those of a static environment as explained in Section III-B. At first we train an off-the-shelf DCNN as introduced in [20], [21] to conduct localization assuming the environment is static. In this regard, we suppose we have a dataset of geo-tagged CSIs that maps the underlying BG exhaustively. To obtain a dataset of geo-tagged ADPs, we transform all CSIs to ADPs using (4). We denote the dataset by Υ which consists of ADPs paired by locations. Then we take the DCNN and train it based on the dataset to conduct the localization task when ADPs are not distorted.

Now, we assume a stream of CSIs are measured consecutively to establish and maintain the link between the user and the BS. H_t denotes the CSI measured at time t , and A_t denotes the corresponding ADP. Primarily, we develop an algorithm to determine whether the measured ADP is distorted or not. In this regard, we pass A_t through DCNN and estimate

the user location. Then we search the dataset and find nearby locations to the estimated location and compare the paired ADPs with the measured ADP, to see if there is at least one ADP among them that is similar to the measured one. To quantitatively measure similarity between two ADPs, we need a similarity metric. In [29], authors introduce the joint angle-delay similarity coefficient (JDASC) and prove that it is a decreasing function of physical distance. We observed that simple normalized correlation between two ADPs does the job as well. Thus, we define normalized correlation \mathcal{S} as

$$\mathcal{S}(\mathbf{A}, \hat{\mathbf{A}}) = \frac{\text{vec}(\mathbf{A}) \cdot \text{vec}(\hat{\mathbf{A}})}{\|\mathbf{A}\|_F \|\hat{\mathbf{A}}\|_F}, \quad (7)$$

where $\mathbf{A}, \hat{\mathbf{A}}$ denote two arbitrary ADPs, $\text{vec}(\cdot)$ denotes an operator that concatenates columns of a matrix into a vector, operation \cdot denotes inner product and $\|\cdot\|_F$ denotes Frobenius norm. If there is at least one ADP from the neighboring locations whose similarity to the measured ADP is more than a predefined threshold (thr_2), we label the ADP as "accurate", otherwise we label it as "distorted". The algorithm for distorted ADP detection is summarized in Algorithm 1. The rationale behind the proposed algorithm stems from our discussion in Section III-A that ADP is highly correlated in the location domain. Since the DCNN is solely trained by accurate ADPs, it will return inaccurate locations when faced with distorted ADPs. Hence, nearby ADPs will not show high similarities with the measured ADP. On the other hand, if the measured ADP is accurate, there will be an ADP in the nearby ADPs that looks very similar to the measured one.

Algorithm 1 Distorted ADP Detection

Require: measured CSI at time t , \mathbf{H}_t ; $\text{thr}_1, \text{thr}_2$

Ensure: \mathbf{H}_t is distorted or accurate

- 1: Convert \mathbf{H}_t to ADP \mathbf{A}_t using (4)
 - 2: Apply \mathbf{A}_t to DCNN and get the location estimation \mathbf{x}_t
 - 3: $\mathbb{X}_t \leftarrow$ find all paired ADPs in the dataset where their tagged locations are closer than thr_1 to \mathbf{x}_t
 - 4: $flag \leftarrow 0$
 - 5: **for** all ADPs $\mathbf{A} \in \mathbb{X}_t$ **do**
 - 6: $s \leftarrow \mathcal{S}(\mathbf{A}, \mathbf{A}_t)$
 - 7: **if** $s > \text{thr}_2$ **then**
 - 8: $flag \leftarrow 1$
 - 9: **end if**
 - 10: **end for**
 - 11: **if** $flag == 1$ **then**
 - 12: **return** accurate
 - 13: **else**
 - 14: **return** distorted
 - 15: **end if**
-

If the measured ADP is accurate, we can simply use DCNN for localization. On the other hand, if it is distorted, we propose to use WKNN along with a video frame prediction algorithm to recover the true ADP and conduct localization. Based on our discussion in Sections III-A and IV, time-series of accurate ADPs are highly correlated temporally. Thus, given time-series of accurate ADPs before facing a distorted ADP, we try to predict the next frame of the time-series using a predictive recurrent neural network (PredRNN). PredRNN is

a frame prediction algorithm that tries to learn dependencies between consecutive frames and uses this knowledge to predict the next frame of the sequence. Frame prediction is a challenging problem in CV and several algorithms have been published to address it [31], [32]. We chose PredRNN mainly because it shows promising results on the radar echo dataset. The detailed discussion about PredRNN can be found in [33]. In this work, we assume that we have a sequence of past accurate ADPs with length $f \in \mathbb{N}$ at time t , $\mathbf{A}_{t-fT_s}, \dots, \mathbf{A}_{t-T_s}$ denoted by $\bar{\mathbf{A}}_t$. We train the network based on a dataset of random walks which we generate using Υ . In Section VI-C, we will describe how we generate the moving dataset, the PredRNN structure and how we train it, in details.

After detecting a distorted ADP, we pass \mathbf{A}_t through the trained PredRNN to predict the accurate ADP denoted by $\hat{\mathbf{A}}_t$. Next, we pass $\hat{\mathbf{A}}_t$ through DCNN to obtain an initial estimation of the user location $\hat{\mathbf{x}}_t$. In addition to frame prediction, in light of the fact that ADPs are highly correlated in location domain, we can take the last location estimation based on the last accurate ADP and find nearby locations in the database and use them to reach a better location estimation and recover the true ADP. To clarify, if some paths in the ADP get blocked or added, the remaining paths pose correlation with nearby ADPs. Thus, using the similarity criteria (7), we can extract the residual similarities between the distorted ADP and nearby ADPs. Moreover, we calculate the similarity between the distorted ADP and the predicted one. Now we are able to combine nearby locations and ADPs and the estimated location and ADP via a WKNN algorithm to obtain a better location estimation and recover ADP. Weights of WKNN can be determined directly from calculated similarities. Hence, the location and the true ADP can be estimated as

$$\mathbf{x}_t = \sum_{x \in \mathcal{N}} w_x \mathbf{x}; \quad \bar{\mathbf{A}}_t = \sum_{x \in \mathcal{N}} w_x \mathbf{A}_x, \quad (8)$$

where \mathbf{x}_t denotes the estimated location and $\bar{\mathbf{A}}_t$ denotes the recovered ADP, \mathbf{A}_x is ADP at location \mathbf{x} , \mathcal{N} denotes union of the set of nearby locations added by the predicted location, and w_x is the weight, given by

$$w_x = \frac{\mathcal{S}(\mathbf{A}_t, \mathbf{A}_x)}{\sum_{\mathbf{A} \in \mathcal{A}} \mathcal{S}(\mathbf{A}_t, \mathbf{A})}, \quad (9)$$

where \mathcal{A} denotes the set of ADPs corresponding to locations in \mathcal{N} . Finally, we can estimate the user location at time t (denoted by \mathbf{x}_t) and recover the ADP ($\bar{\mathbf{A}}_t$) which can be used for future location estimations. Algorithm 2 summarizes the proposed algorithm for ADP recovery and location estimation. Moreover, Fig. 3 summarizes the end-to-end DyLoc localization framework.

VI. SIMULATIONS

In this section, the performance of our proposed localization framework for an indoor and an outdoor environments is studied. In Section VI-A, we present the dataset that we used for static environment fingerprinting. We define the structure of the DCNN and how to train it in Section VI-B. Then, we clarify how we generate the moving dataset using the static

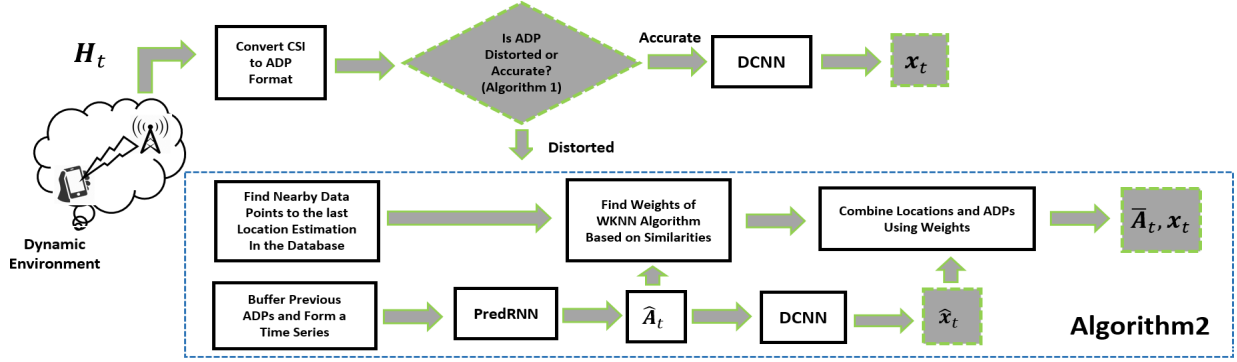


Fig. 3: Block Diagram of the proposed localization framework DyLoc.

Algorithm 2 Location Estimation When ADP Is Distorted

Require: time-series of accurate ADPs $\mathcal{A}_t : \mathbf{A}_{t-T_s f}, \dots, \mathbf{A}_{t-T_s}$
 distorted ADP \mathbf{A}_t
 geo-tagged ADP dataset Υ
 the previous estimated location \mathbf{x}_{t-T_s}
 thr_3

Ensure: The recovered ADP $\bar{\mathbf{A}}_t$, and location estimation \mathbf{x}_t

- 1: **Frame prediction**
- 2: Apply \mathcal{A}_t to PredRNN and get the predicted ADP $\hat{\mathbf{A}}_t$
- 3: Apply $\hat{\mathbf{A}}_t$ to DCNN and get the location estimation $\hat{\mathbf{x}}_t$
- 4: **WKNN**
- 5: $\mathcal{N} \leftarrow$ find all data points in the database which their locations are closer than thr_3 to \mathbf{x}_{t-T_s}
- 6: $\mathcal{N}_A \leftarrow$ paired ADPs of locations in \mathcal{N}
- 7: $\mathcal{N} \leftarrow \mathcal{N} \cup \hat{\mathbf{A}}_t$
- 8: $\mathcal{N}_A \leftarrow \mathcal{N}_A \cup \hat{\mathbf{A}}_t$
- 9: $\mathbf{x}_t \leftarrow \sum_{x \in \mathcal{N}} w_x \mathbf{x}_x$; $w_x = \frac{\mathcal{S}(\mathbf{A}_t, \mathbf{A}_x)}{\sum_{\mathbf{A} \in \mathcal{N}_A} \mathcal{S}(\mathbf{A}_t, \mathbf{A})}$
- 10: $\bar{\mathbf{A}}_t \leftarrow \sum_{x \in \mathcal{N}} w_x \mathbf{A}_x$
- 11: **return** $\bar{\mathbf{A}}_t, \mathbf{x}_t$

dataset in Section VI-A1. Further, we explain the structure of the PredRNN and how we trained it. Next, we express dynamic scenarios generated to test the performance of DyLoc. Finally, in Section VI-D we dive deep into evaluating the performance of DyLoc for various dynamic scenarios and compare it with the state-of-the-art.¹

A. Static Datasets

In this work, we use DeepMIMO dataset to generate CSI datasets in static environments². Thus far, DeepMIMO has introduced for one outdoor and two indoor environments. We picked one indoor and one outdoor environments for our simulations.

1) *Outdoor Environment*: To generate an outdoor environment we select DeepMIMO outdoor scenario number 1 (O1) at 3.5 GHz band. "O1" is an urban environment of two streets and one intersection. We suppose only BS number 2 (BS2) is working and it has been equipped with a ULA with $N_t = 64$ antennas aligned with y-axis. We set the OFDM bandwidth to 10 MHz and $N_c = 64$. We also set the number of paths to

¹The authors release their codes in the following link "https://github.com/FarzamHejazik/DyLoc".

²http://www.deepmimo.net/

25. Furthermore, we only generate a dataset for R1 to R1100 (Rows 1 to 1100, show locations of data points in DeepMIMO), therefore the dataset constitutes of 199100 data points. Table I summarizes the dataset parameters.

2) *Indoor Environment*: We picked DeepMIMO indoor scenario number 3 "I3" at 60 GHz to emulate an indoor environment. "I3" simulates a $10m \times 11m$ conference room and its hallway. We assume only access point number 2 (BS2) is working. Other parameters that set up the indoor propagation environment are reflected in Table I.

B. DCNN Setup

As we explained in Section I, in [21] two different DCNNs have been introduced to pursue localization using ADPs. We refer to the first setup that utilizes a regression network as DCNN and the second setup that uses a classification network along with WKNN as DCNN+WKNN. In our work, we train the DCNN to learn the background scattering environment as a part of DyLoc as described in Section V. We also compare the performance of DCNN and DCNN+WKNN with DyLoc.

TABLE I: "O1" and "I3" DeepMIMO datasets' parameters

Parameter	Outdoor Scenario (O1)	Indoor Scenario (I3)
Frequency Band	3.5 GHz	60 GHz
Bandwidth	10 MHz	0.5 GHz
BS	BS2	BS2
Antenna	ULA	ULA
Antenna Elements (N_t)	64	32
Antenna Alignment	y-axis	x-axis
Sub-carrier Number (N_c)	64	32
Path Number	25	25
Locations	R1 to R1100	R1 to R550

1) *Outdoor Environment*: Based on the architecture presented in [21], we choose the parameters presented in Table II for the DCNN setup. We use Max-pooling for pooling layers with size 2×2 and ReLU for activation function. We set training epochs to 500. The setup for the classification network in DCNN+WKNN is the same as DCNN while we add a Softmax layer to the network to conduct classification. Defining area of interest as the set of all locations in the dataset, we assume a 18×55 grid on the area of interest (18 equally-spaced segments in the x-direction and 55 segments

in the y-direction). The classification network is trained to determine to which cell of the grid an input ADP belongs. Then using a WKNN technique with $k = 3$ we estimate the location.

2) *Indoor Environment*: Parameters setup in Section VI-A2 results in 32×32 ADP images in this scenario. We train a 5-layer regression DCNN with parameters as in Table II to learn the underlying propagation environment. The number of training epochs in this simulation is set to 200. The classification CNN setup in DCNN+WKNN technique is the same as the DCNN setup. Similar to the outdoor environment we assume a 18×55 grid on the area of interest. We also set $k = 3$ for the WKNN technique.

TABLE II: DCNN setup for "O1" and "I3"

Layer	Kernel Size (O1)	Kernel Number (O1)	Kernel Size (I3)	Kernel Number (I3)
1	$32 \times 32 \times 1$	2	$16 \times 16 \times 1$	4
2	$16 \times 16 \times 2$	4	$8 \times 8 \times 4$	8
3	$8 \times 8 \times 4$	8	$7 \times 7 \times 8$	16
4	$7 \times 7 \times 8$	16	$5 \times 5 \times 16$	32
5	$5 \times 5 \times 16$	32	$3 \times 3 \times 32$	64
6	$3 \times 3 \times 32$	64		

C. Moving Dataset and PredRNN Setup

To train PredRNN and to emulate dynamic scenarios, we needed moving datasets. We generated moving datasets utilizing static datasets introduced in the previous section. Since the static datasets define the propagation environment thoroughly, they can be used to form dynamic datasets by stacking adjacent locations and paired ADPs. Both "O1" and "I3" datasets assume a grid on the corresponding environment ("O1" assumes a 20 cm distance between two adjacent grid points and "I3" assumes grid of 1 cm apart). We take advantage of the underlying grid and form our moving dataset. To initialize each movement, we suppose the user is randomly placed on one of the grid points. Then at each step of the movement the user moves to one of the adjacent grid points.

We assume the movement continues for f consecutive steps. Next, we stacked all locations and paired ADPs together to form and save one sequence. We consider 2 modes for user random walks:

- **Mode 1:** User chooses its direction only at the first time-step and continues the same direction in the following time-steps. If the user reaches the boundaries of the environment, the user chooses another direction from possible remaining directions randomly.
- **Mode 2:** User goes for a complete random walk and at each time-step chooses a new direction.

To train PredRNN, we generated the whole dataset based on mode 1 movements since we expect that PredRNN is not able to predict ADPs stem from fully random walks. Thus, we generated 10000 sequences each with length 11. We employed the PredRNN presented in [33] with the same setup and parameters. We fed the first 10 ADP frames to the network and optimized the network to predict the 11th ADP; so we do not use the location sequence for training, we only make use of

the paired ADPs. Eventually, we expect the trained PredRNN is capable of predicting the next ADP in the sequence, given the 10 last accurate ADPs.

1) *Dynamic Test Scenarios*: To evaluate the performance of the proposed DyLoc algorithm, we generate 1000 sequences of length 20 for each of the indoor and the outdoor environments. Half of these sequences is generated based on Mode 1 movements and half of them based on Mode 2. We assume the first 10 frames of each sequence consist of accurate ADPs and FG does not affect them. On the other hand, we assume the last 10 frames of each sequence are distorted based on one of the following scenarios:

- **LOS Blockage:** we assume that the most powerful path between the BS and the user gets blocked, thus we eliminate this path from all 10 ADP frames.
- **NLOS Blockage:** we assume that the second most powerful path between the BS and the user gets blocked, thus we wipe out this path from all 10 ADP frames.
- **NLOS Addition:** we add a path 6dB weaker than the strongest path arbitrarily located in the ADP image to all 10 ADP frames.

We inspect DyLoc performance for the above 3 scenarios for both "O1" and "I3" environments and compare it with the state-of-the-art DCNN and DCNN+WKNN algorithm [21].

D. Results and Discussion

In this section, we present the performance of DyLoc for the scenarios introduced in Section VI-C for the outdoor environment "O1" and the indoor environment "I3".

1) *Outdoor Environment*: Table III summarizes root mean square error (RMSE) of location estimation for the distorted frames for the 3 scenarios using DyLoc and compares it with DCNN and DCNN+WKNN. For the first 10 accurate frames, the RMSE for all scenarios using DCNN and DCNN+WKNN is 19 cm and 14.5 cm, respectively. Since DyLoc uses the same DCNN when frames are accurate, the DyLoc accuracy is 19 cm. However, when the frames are distorted, DCNN error proliferates to more than 20 m when LOS is blocked, more than 10 m when NLOS is added, and more than 7.5 m when NLOS is blocked. This huge surge in error is because DCNN has not been trained for localization based on distorted ADPs. Moreover, DCNN error is the highest when LOS is blocked. Since the outdoor environment is not a rich scattering environment and generally there are 2-3 paths between the BS and the user, the LOS path contains the most valuable information in the ADP, so if it is blocked, the DCNN loses its most important clue for localization. When NLOS paths are distorted, the effect of NLOS addition is more than NLOS blockage since we assume a very strong path is added to the ADP. The DCNN+WKNN performance is even worse than DCNN facing distorted ADPs and the error is more than 180 m when LOS is blocked, more than 30 m when NLOS is added, and more than 50 m when NLOS is blocked. Since the classification network cannot find the correct cell that the distorted ADP belongs to, the WKNN layer does not perform well and the performance plunges drastically.

TABLE III: Location estimation RMSE in meter of the last 10 frames of the time-series employing DyLoc, DCNN [21], DCNN+WKNN [21], and PredRNN [33] for LOS blockage, NLOS blockage, NLOS addition scenarios at outdoor environment "O1" and outdoor environment "I3". PredRNN error shows location estimation error of the predictive arm of DyLoc.

		RMSE(m)	Frame Number									
			11	12	13	14	15	16	17	18	19	20
Scenario O1	LOS Blockage	DyLoc	0.37	0.53	0.69	0.85	1.00	1.14	1.29	1.43	1.57	1.71
		DCNN	25.55	25.14	25.51	25.01	25.18	24.58	25.17	25.72	24.11	24.96
		DCNN + WKNN	181.66	179.30	178.88	178.90	175.11	178.90	183.42	176.93	180.52	176.00
		PredRNN	2.05	1.96	2.32	2.45	2.56	2.72	2.88	3.05	3.24	3.56
	NLOS Blockage	DyLoc	0.30	0.38	0.45	0.52	0.58	0.65	0.71	0.78	0.83	0.89
		DCNN	10.15	10.69	10.95	11.05	10.60	11.23	11.06	10.95	10.98	10.65
		DCNN + WKNN	36.17	34.66	34.52	34.45	38.95	35.32	36.86	36.23	35.72	39.38
		PredRNN	2.05	2.09	2.16	2.16	2.21	2.22	2.21	2.26	2.28	2.34
	NLOS Addition	DyLoc	0.30	0.42	0.53	0.63	0.72	0.82	0.91	0.99	1.08	1.16
		DCNN	15.09	15.09	15.26	15.44	15.00	15.21	14.80	15.36	15.12	15.66
		DCNN + WKNN	55.86	57.43	55.06	55.45	54.41	56.40	53.86	54.69	53.70	55.59
		PredRNN	2.05	2.23	2.39	2.38	2.38	2.40	2.44	2.48	2.51	2.57
Scenario I3	LOS Blockage	DyLoc	0.04	0.04	0.04	0.05	0.05	0.06	0.06	0.07	0.07	0.08
		DCNN	0.93	0.93	0.93	0.92	0.93	0.92	0.93	0.93	0.93	0.93
		DCNN + WKNN	2.02	2.00	2.04	2.03	1.99	2.01	2.03	1.99	2.00	1.99
		PredRNN	0.15	0.16	0.16	0.16	0.17	0.17	0.17	0.17	0.17	0.17
	NLOS Blockage	DyLoc	0.05	0.05	0.06	0.06	0.07	0.07	0.07	0.08	0.08	0.08
		DCNN	0.47	0.47	0.47	0.48	0.48	0.48	0.47	0.46	0.46	0.47
		DCNN + WKNN	1.12	1.10	1.07	1.11	1.10	1.06	1.11	1.13	1.12	1.10
		PredRNN	0.15	0.16	0.16	0.17	0.17	0.18	0.18	0.18	0.18	0.18
	NLOS Addition	DyLoc	0.04	0.04	0.05	0.05	0.06	0.06	0.07	0.07	0.08	0.08
		DCNN	0.20	0.20	0.20	0.19	0.19	0.19	0.19	0.19	0.19	0.19
		DCNN + WKNN	1.35	1.27	1.33	1.39	1.32	1.36	1.34	1.37	1.33	1.32
		PredRNN	0.15	0.16	0.16	0.17	0.17	0.18	0.18	0.18	0.18	0.18

In contrast to DCNN and DCNN+WKNN, DyLoc performs with high accuracy when faces distorted ADPs. Regarding the TABLE III, as frame number increases the DyLoc error increases. This is totally expected since the prediction error of the previous predicted frames propagates to the next frame and results in a higher error at the next frame. Nevertheless, the error remains less than 1.8 m, 1.2 m, and 0.9 m, for LOS blockage, NLOS addition, and NLOS blockage for all the distorted frames, respectively. These error values show a quite promising performance by DyLoc in the outdoor environment for dynamic scenarios.

Referring to Table III, RMSE of location estimation via the predictive arm of Algorithm 2 (PredRNN) -before incorporating WKNN (\hat{x}_t)- for all distorted frames and for the 3 scenarios are expressed. The error changes between 2.0 m to 2.4 m for the NLOS blockage scenario, 2.0 m to 2.6 m in the NLOS addition scenario, and 2.0 m to 3.6 m in the LOS blockage scenario. The error is increasing with a higher rate when LOS gets blocked since the measured ADP can help us the least to improve our prediction. Moreover, in the LOS blockage scenario, especially when we have only one path between the BS and the user, and it gets blocked (i.e. the connection is lost), \hat{x}_t is our exclusive source of location estimation. Thus, the predictive arm is very crucial for location estimation in the LOS blockage scenario. Additionally, when we incorporate WKNN to form DyLoc, the error values decrease to 0.3 m (frame 11) and 0.89 m (frame 20), 0.3 m (frame 11) and 1.16 m (frame 20), and 0.37 m (frame 11) and 1.71 m (frame 20) for the NLOS Blockage, NLOS addition, and LOS blockage

scenarios, respectively. These results show that the WKNN arm is pretty successful in reducing the total estimation error. Consequently, both WKNN and PredRNN arms are crucial for accurate location estimation and robustness to FG dynamic changes.

2) *Indoor Environment:* Similar to the outdoor environment, we compare DCNN, DCNN+WKNN, and DyLoc algorithms in the indoor environment "I3" for the 3 dynamic scenarios. In contrast to the outdoor environment, the indoor environment is a rich scattering environment and there are several propagation paths between the BS and the user. The RMSE for accurate frames utilizing DCNN is 5 cm and DCNN+WKNN is 4.5 cm. Unlike the outdoor scenario, the indoor scenario DCNN performs much better when NLOS is added to the ADP. This happens because the scattering environment is rich and NLOS addition can be filtered out by DCNN.

As Table III expresses, RSME of DyLoc is less than 8 cm for all scenarios and the performance of DyLoc is very close in these scenarios. This can be justified by the fact that the scattering environment is very rich and the pervasiveness of paths helps DyLoc to obtain a robust location estimation to environment changes. This fact is also reflected in the RSME of PredRNN. Again, the performance of PredRNN is pretty close in the 3 scenarios and the error changes between 15 cm to 18 cm. Interestingly, it seems that the PredRNN performs better in predicting the LOS path position in the ADP rather than the NLOS paths. We may explain this phenomena by the fact that the LOS path is stronger than the NLOS paths

and the predictive network could learn to predict its location better than weaker NLOS paths. Thus, centimeter accuracy in the indoor environments is achievable using DyLoc.

VII. CONCLUSION

We have introduced a novel framework to address data-driven localization in dynamic environments. We have discussed that proposed deep learning algorithms in the literature fail to tackle localization in dynamic environments since they are principally dependent on prolonged tasks of data gathering and network training. Taking advantage of a meaningful representation of communication channel, we have devised an algorithm to discover dynamic changes in the propagation environment. Based on that, we have developed DyLoc to perform localization in time-varying environments. We have showcased the performance of DyLoc in indoor and outdoor environments. Our results have shown that DyLoc is able to pursue localization accurately in the both environments. Moreover, simulation results have revealed that when the number of multipath increases, DyLoc becomes more robust to time-varying changes.

ACKNOWLEDGMENT

This work is supported by the National Science Foundation under Grant No. CCF-1718195.

REFERENCES

- [1] Ahmed Alkhateeb, "Deepmimo: A generic deep learning dataset for millimeter wave and massive mimo applications," *arXiv preprint arXiv:1902.06435*, 2019.
- [2] Iris A Junglas and Richard T Watson, "Location-based services," *Communications of the ACM*, vol. 51, no. 3, pp. 65, 2008.
- [3] I. Guvenc and C. Chong, "A survey on toa based wireless localization and nlos mitigation techniques," *IEEE Communications Surveys & Tutorials*, vol. 11, no. 3, pp. 107–124, 2009.
- [4] F. Zafari, A. Gkelias, and K. K. Leung, "A survey of indoor localization systems and technologies," *IEEE Communications Surveys & Tutorials*, vol. 21, no. 3, pp. 2568–2599, 2019.
- [5] Mislav Zane, Markus Rupp, and Stefan Schwarz, "Performance investigation of angle of arrival based localization," in *WSA 2020; 24th International ITG Workshop on Smart Antennas*. VDE, 2020, pp. 1–4.
- [6] Sebastian Sadowski and Petros Spachos, "Rssi-based indoor localization with the internet of things," *IEEE Access*, vol. 6, pp. 30149–30161, 2018.
- [7] Zhenhua Ma and KC Ho, "Toa localization in the presence of random sensor position errors," in *2011 IEEE International Conference on Acoustics, Speech and Signal Processing (ICASSP)*. IEEE, 2011, pp. 2468–2471.
- [8] Regina Kaune, Julian Hörst, and Wolfgang Koch, "Accuracy analysis for tdoa localization in sensor networks," in *14th International Conference on Information Fusion*. IEEE, 2011, pp. 1–8.
- [9] Farzam Hejazi, Mohsen Joneidi, and Nazanin Rahnavard, "A tensor-based localization framework exploiting phase interferometry measurements," in *2020 IEEE International Radar Conference (RADAR)*. IEEE, 2020, pp. 554–559.
- [10] Farzam Hejazikookamari, Yaser Norouzi, Elham Sadat Kashani, and Mohammad Mahdi Nayebe, "A novel method to detect and localize lpi radars," *IEEE Transactions on Aerospace and Electronic Systems*, vol. 55, no. 5, pp. 2327–2336, 2018.
- [11] F Hejazi, MM Khalili, Y Norouzi, and MM Nayebe, "A new pseudolinear solution to bearing-only tracking," in *2013 IEEE Radar Conference (RadarCon13)*. IEEE, 2013, pp. 1–4.
- [12] F Hejazi, Y Norouzi, and MM Nayebe, "Sar processing to localize lpi radars," in *2014 International Radar Conference*. IEEE, 2014, pp. 1–4.
- [13] F Hejazi, Yaser Norouzi, and Mohammad Mehdi Nayebe, "Lower bound of error in aoa based passive source localization using single moving platform," in *East-West Design & Test Symposium (EWDTS 2013)*. IEEE, 2013, pp. 1–4.
- [14] Farzam Hejazi Kookamari, Yaser Norouzi, and Mohammad Mahdi Nayebe, "Using a moving aerial platform to detect and localise a low probability of intercept radar," *IET Radar, Sonar & Navigation*, vol. 11, no. 7, pp. 1062–1069, 2017.
- [15] Chaoyun Zhang, Paul Patras, and Hamed Haddadi, "Deep learning in mobile and wireless networking: A survey," *IEEE Communications Surveys & Tutorials*, vol. 21, no. 3, pp. 2224–2287, 2019.
- [16] Faheem Zafari, Athanasios Gkelias, and Kin K Leung, "A survey of indoor localization systems and technologies," *IEEE Communications Surveys & Tutorials*, vol. 21, no. 3, pp. 2568–2599, 2019.
- [17] Hengtao He, Shi Jin, Chao-Kai Wen, Feifei Gao, Geoffrey Ye Li, and Zongben Xu, "Model-driven deep learning for physical layer communications," *IEEE Wireless Communications*, vol. 26, no. 5, pp. 77–83, 2019.
- [18] Erik G Larsson, Ove Edfors, Fredrik Tufvesson, and Thomas L Marzetta, "Massive mimo for next generation wireless systems," *IEEE communications magazine*, vol. 52, no. 2, pp. 186–195, 2014.
- [19] Volker Jungnickel, Konstantinos Manolakis, Wolfgang Zirwas, Berthold Panzner, Volker Braun, Moritz Lossow, Mikael Sternad, Rikke Apelfröjd, and Tommy Svensson, "The role of small cells, coordinated multipoint, and massive mimo in 5g," *IEEE communications magazine*, vol. 52, no. 5, pp. 44–51, 2014.
- [20] Joao Vieira, Erik Leitinger, Muris Sarajlic, Xuhong Li, and Fredrik Tufvesson, "Deep convolutional neural networks for massive mimo fingerprint-based positioning," in *2017 IEEE 28th Annual International Symposium on Personal, Indoor, and Mobile Radio Communications (PIMRC)*. IEEE, 2017, pp. 1–6.
- [21] Xiaoyu Sun, Chi Wu, Xiqi Gao, and Geoffrey Ye Li, "Fingerprint-based localization for massive mimo-ofdm system with deep convolutional neural networks," *IEEE Transactions on Vehicular Technology*, vol. 68, no. 11, pp. 10846–10857, 2019.
- [22] Paul Ferrand, Alexis Decurninge, and Maxime Guillaud, "Dnn-based localization from channel estimates: Feature design and experimental results," *arXiv preprint arXiv:2004.00363*, 2020.
- [23] Sibren De Bast and Sofie Pollin, "Mamimo csi-based positioning using cnns: Peeking inside the black box," *arXiv preprint arXiv:2003.04581*, 2020.
- [24] Rashmika Nawaratne, Daminda Alahakoon, Daswin De Silva, and Xinghuo Yu, "Spatiotemporal anomaly detection using deep learning for real-time video surveillance," *IEEE Transactions on Industrial Informatics*, vol. 16, no. 1, pp. 393–402, 2019.
- [25] Hyomin Choi and Ivan V Bajić, "Deep frame prediction for video coding," *IEEE Transactions on Circuits and Systems for Video Technology*, 2019.
- [26] Waqas Sultani, Chen Chen, and Mubarak Shah, "Real-world anomaly detection in surveillance videos," in *Proceedings of the IEEE Conference on Computer Vision and Pattern Recognition*, 2018, pp. 6479–6488.
- [27] Anum Ali, Nuria González-Prelcic, and Robert W Heath, "Millimeter wave beam-selection using out-of-band spatial information," *IEEE Transactions on Wireless Communications*, vol. 17, no. 2, pp. 1038–1052, 2017.
- [28] Ahmed Alkhateeb and Robert W Heath, "Frequency selective hybrid precoding for limited feedback millimeter wave systems," *IEEE Transactions on Communications*, vol. 64, no. 5, pp. 1801–1818, 2016.
- [29] Xiaoyu Sun, Xiqi Gao, Geoffrey Ye Li, and Wei Han, "Single-site localization based on a new type of fingerprint for massive mimo-ofdm systems," *IEEE Transactions on Vehicular Technology*, vol. 67, no. 7, pp. 6134–6145, 2018.
- [30] Yuan Shen and Moe Z Win, "On the use of multipath geometry for wideband cooperative localization," in *GLOBECOM 2009-2009 IEEE Global Telecommunications Conference*. IEEE, 2009, pp. 1–6.
- [31] Xiaodan Liang, Lisa Lee, Wei Dai, and Eric P Xing, "Dual motion gan for future-flow embedded video prediction," in *Proceedings of the IEEE International Conference on Computer Vision*, 2017, pp. 1744–1752.
- [32] Wen Liu, Weixin Luo, Dongze Lian, and Shenghua Gao, "Future frame prediction for anomaly detection—a new baseline," in *Proceedings of the IEEE Conference on Computer Vision and Pattern Recognition*, 2018, pp. 6536–6545.
- [33] Yunbo Wang, Mingsheng Long, Jianmin Wang, Zhifeng Gao, and S Yu Philip, "Predrnn: Recurrent neural networks for predictive learning using spatiotemporal lstms," in *Advances in Neural Information Processing Systems*, 2017, pp. 879–888.